

## Supporting Information

### Construction of Bi-based Amorphous/Crystalline Heterostructures for Efficient Potassium Ion Storage

Hankun Yang<sup>#a</sup>, Xiaoqing Zhang<sup>#a</sup>, Wei Li<sup>a</sup>, Yufang Chen<sup>\*b</sup>, Xiaolei Tang<sup>a</sup>, Ying Wu<sup>a</sup>,  
Qiliang Wei<sup>\*ac</sup>, Xianyou Wang<sup>a</sup>, Hongbo Shu<sup>\*a</sup>

<sup>a</sup> National Base for International Science & Technology Cooperation, Hunan Province Key Laboratory for Electrochemical Energy Storage and Conversion, School of Chemistry, Xiangtan University, Xiangtan 411105, China;

<sup>b</sup> College of Aerospace Science and Engineering, National University of Defense Technology, Changsha 410000, China

<sup>c</sup> Institute of Micro/Nano Materials and Devices, Ningbo University of Technology, Ningbo, 315211, P.R. China

<sup>#</sup>These authors contributed equally to this work.

#### *Characterization of the materials:*

The crystal structure of the was examined by X-ray diffraction (XRD, Rigaku, Ultima IV with D/teX Ultra with CuK $\alpha$  radiation). The morphological and detailed structure characterization was investigated by scanning electron microscopy (SEM, JSM-6610L, Japan) and transmission electron microscopy (TEM, FEI TECNAI G2 F20, America). The surface elemental states of as-synthesized materials were characterized by X-ray photoelectron spectra (XPS, Kratos Axis Ultra DLD, Japan).

#### *Electrochemical Measurements:*

The CR2032-type cells were assembled in the glove box fulfilled by argon. The working electrodes were prepared by mixing the as-prepared products, super P, and PVDF at a weight ratio of 7:2:1. The slurry was casted onto the Cu foil and completely

---

\* Corresponding author: Tel.: +86 73158292060; fax: +86 73158292061.

Email: [hongboshu@xtu.edu.cn](mailto:hongboshu@xtu.edu.cn) (H. Shu), [chenyufang@nudt.edu.cn](mailto:chenyufang@nudt.edu.cn) (Y. Chen), [qiliang.wei@nbut.edu.cn](mailto:qiliang.wei@nbut.edu.cn) (Q. Wei)

dried in a vacuum oven at 50 °C overnight. The average mass loading was about 1.2-1.4 mg cm<sup>-2</sup>. For half-cell testing, K slice was used as the counter electrode, the glass fiber film (Whatman GF/D) was employed as a separator and the electrolyte was composed of 3.0 M KFSI in DME. The galvanostatic discharge-charge tests were measured on the battery testing systems (Neware, Shenzhen). Cyclic voltammetry (CV) and EIS measurements were performed on a CHI660E electrochemical workstation (ChenHua, Shanghai).

*Theoretical Computation:*

The Vienna Ab Initio Simulation Package was used to implement all the DFT calculations.<sup>1</sup> The exchange-correlation interaction between electrons was described by the generalized gradient approximation (GGA) in the strategy of Perdew-Burke-Ernzerhof (PBE) functional. A cutoff energy of 520 eV was applied for the plane-wave expansion of the electronic wave functions. The self-consistency field calculations were conducted with an energy convergence of 10<sup>-4</sup> eV and force convergence of 10<sup>-2</sup> eV/Å.<sup>2</sup> For all of the surfaces explored, the Brillion-zone integration was sampled by adopting a 3×3×1 Gamma-centered k-point mesh. Bi<sub>2</sub>S<sub>3</sub> (211), and Bi<sub>2</sub>O<sub>3</sub> (200) surfaces were applied as stable surfaces for adsorption calculations.

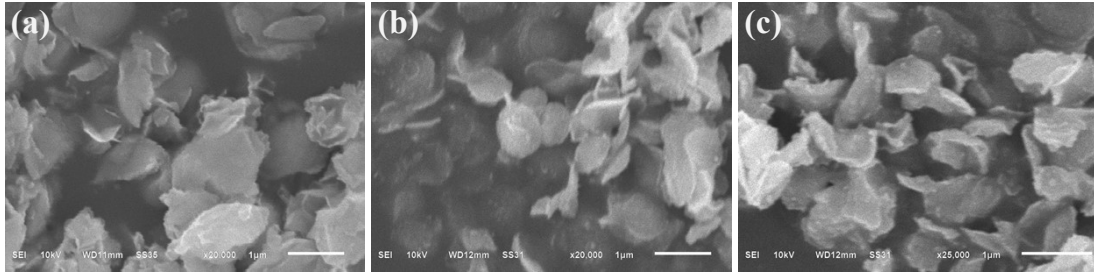


**Figure S1.** SEM image of a)  $c\text{-Bi}_2\text{O}_3$ , b)  $c\text{-Bi}_2\text{S}_3/c\text{-Bi}_2\text{O}_3$ , and c)  $a\text{-Bi}_2\text{S}_3/c\text{-Bi}_2\text{O}_3$ .

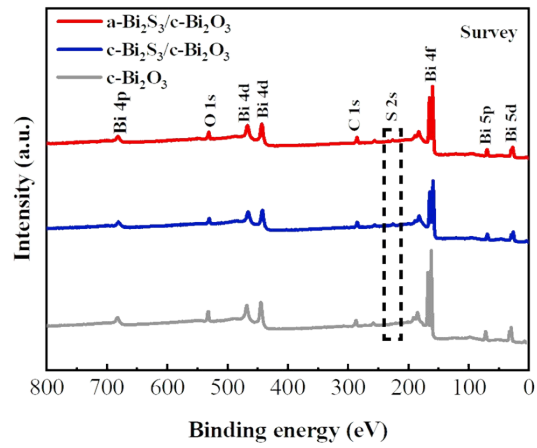


**Figure S2.** XPS survey spectrum of  $a\text{-Bi}_2\text{S}_3/c\text{-Bi}_2\text{O}_3$ ,  $c\text{-Bi}_2\text{S}_3/c\text{-Bi}_2\text{O}_3$ , and  $c\text{-Bi}_2\text{O}_3$ .

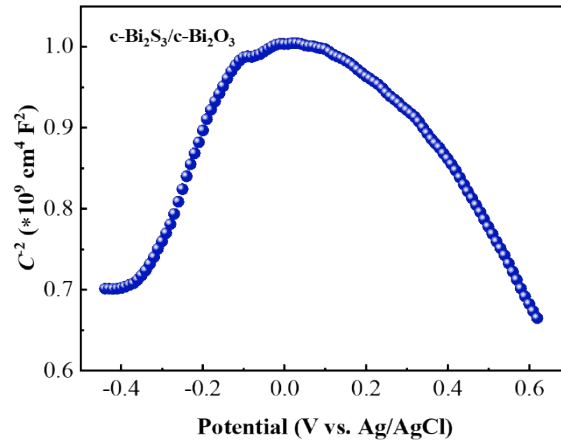


**Figure S3.** Mott-Schottky plot.

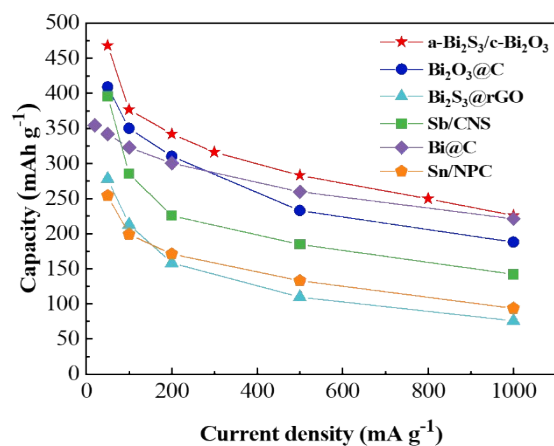


**Figure S4.** Rate performance of a-Bi<sub>2</sub>S<sub>3</sub>/c-Bi<sub>2</sub>O<sub>3</sub> electrode compared with those of the previously reported alloy anodes for KIBs.

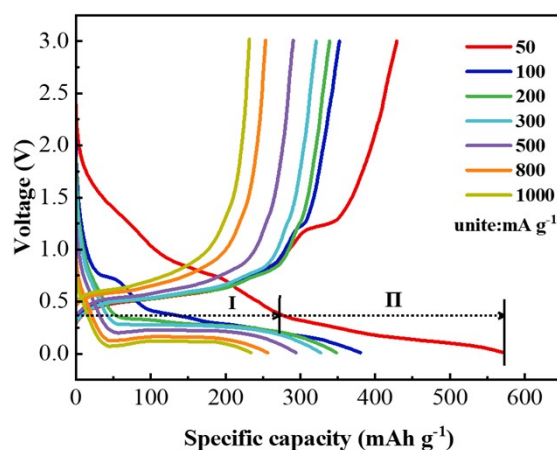


**Figure S5.** Discharge capacity from the embedding/conversion plateau (denoted as I), alloying plateau (denoted as II).

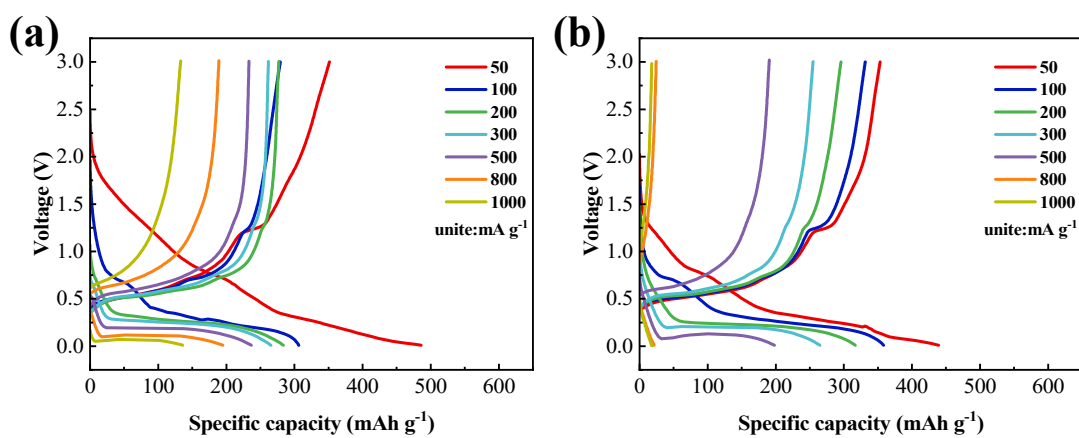


**Figure S6.** Galvanostatic charge-discharge profiles of a) c-Bi<sub>2</sub>S<sub>3</sub>/c-Bi<sub>2</sub>O<sub>3</sub> and b) c-Bi<sub>2</sub>O<sub>3</sub> at various rates.

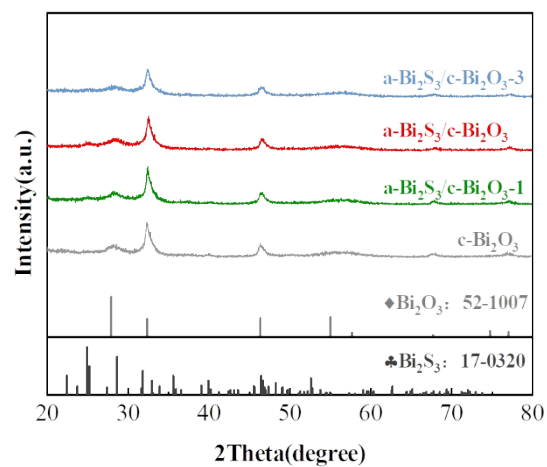


**Figure S7.** XRD pattern with different degrees of sulfidation.

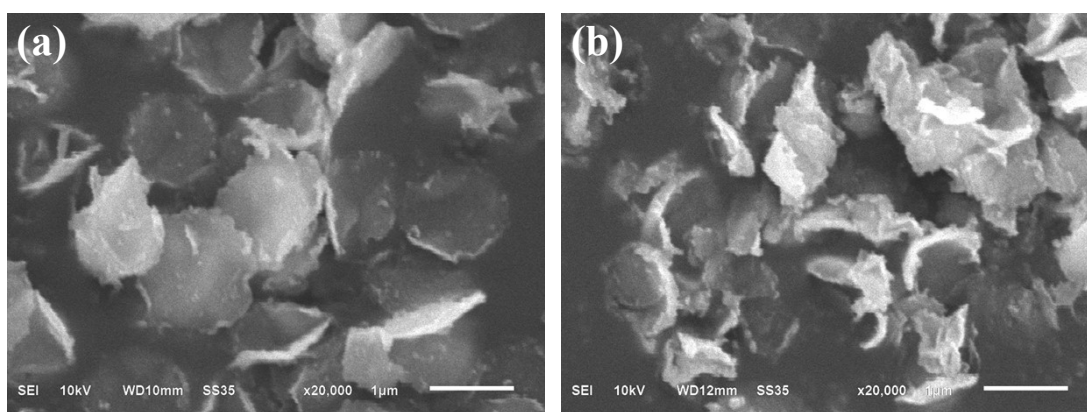


**Figure S8.** SEM image of a,b) a-Bi<sub>2</sub>S<sub>3</sub>/c-Bi<sub>2</sub>O<sub>3</sub>-1 and a-Bi<sub>2</sub>S<sub>3</sub>/c-Bi<sub>2</sub>O<sub>3</sub>-3.

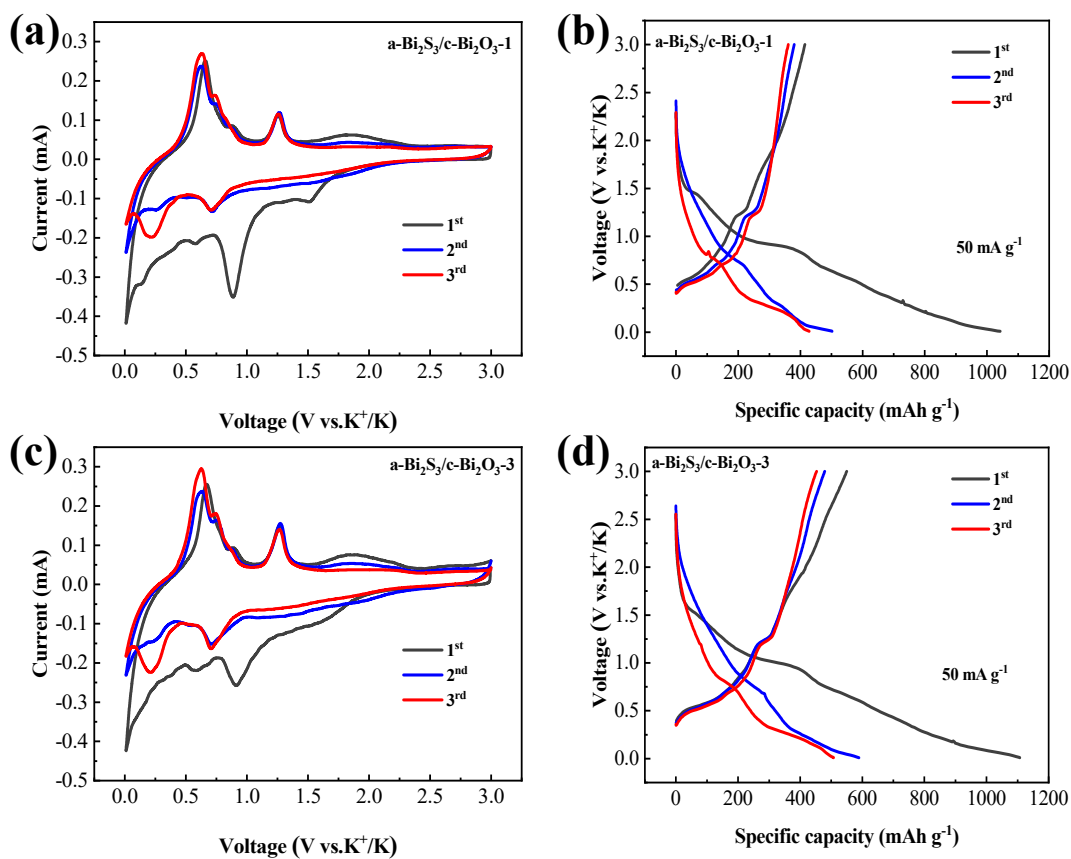


**Figure S9.** a,c) CV curves of a-Bi<sub>2</sub>S<sub>3</sub>/c-Bi<sub>2</sub>O<sub>3</sub>-1 and a-Bi<sub>2</sub>S<sub>3</sub>/c-Bi<sub>2</sub>O<sub>3</sub>-3 at 0.1 mV s<sup>-1</sup>. b,d) Charge/discharge profiles of a-Bi<sub>2</sub>S<sub>3</sub>/c-Bi<sub>2</sub>O<sub>3</sub>-1 and a-Bi<sub>2</sub>S<sub>3</sub>/c-Bi<sub>2</sub>O<sub>3</sub>-3 at 50 mA g<sup>-1</sup>.

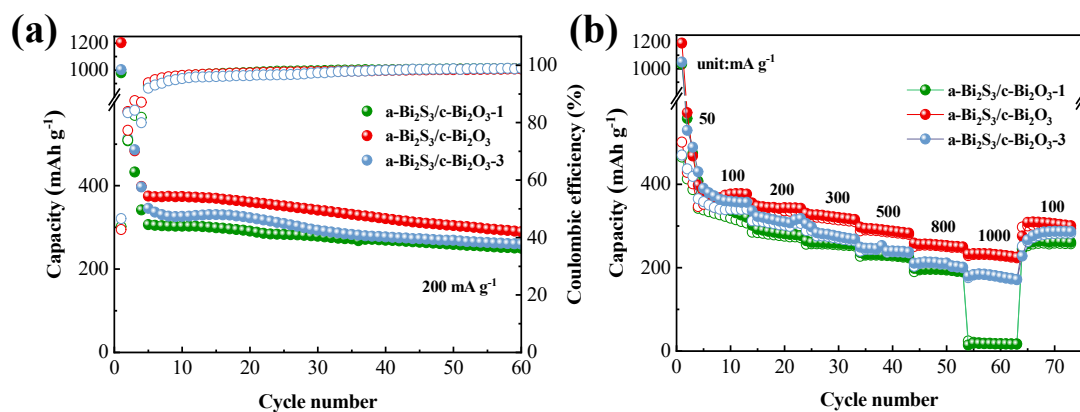


**Figure S10.** a) Cycling performance at 200 mA g<sup>-1</sup>. b) Rate capability.

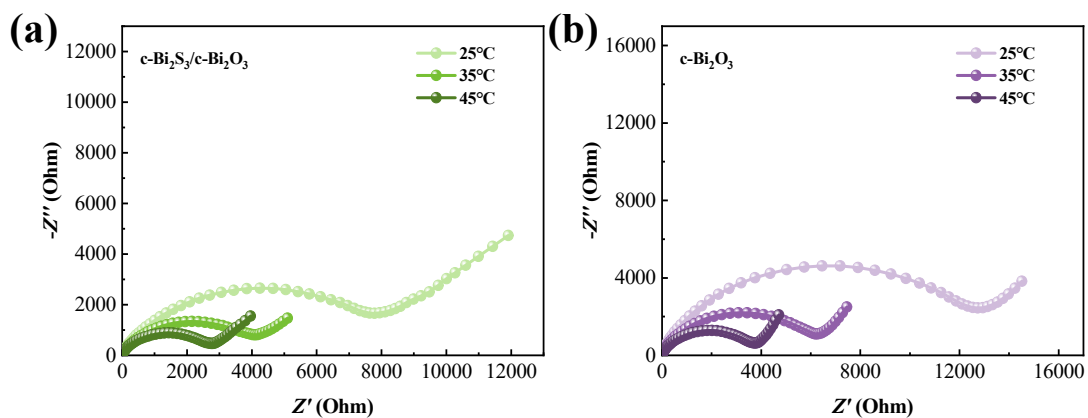


**Figure S11.** EIS curves of a)  $c\text{-Bi}_2\text{S}_3/c\text{-Bi}_2\text{O}_3$  and b)  $c\text{-Bi}_2\text{O}_3$  at different temperatures.

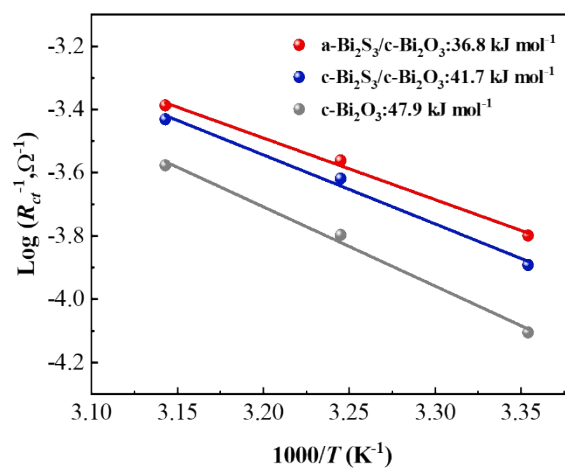


**Figure S12.** The comparison of activation energies.

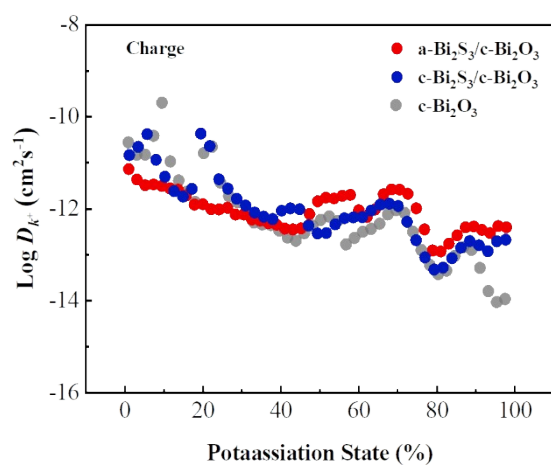


**Figure S13.** Calculated  $\text{K}^+$  diffusion coefficient at different potassiation states during the charging

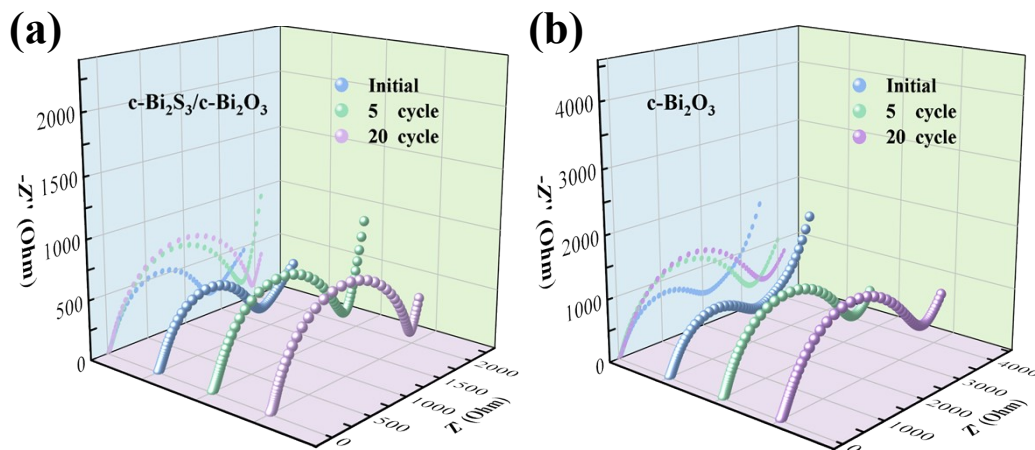


**Figure S14.** EIS curves of a)  $c\text{-Bi}_2\text{S}_3/c\text{-Bi}_2\text{O}_3$  and b)  $c\text{-Bi}_2\text{O}_3$  electrodes after different cycles at  $300 \text{ mA g}^{-1}$ .

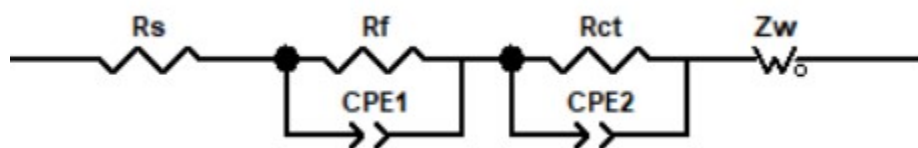


**Fig S15.** The equivalent circuit of Nyquist.

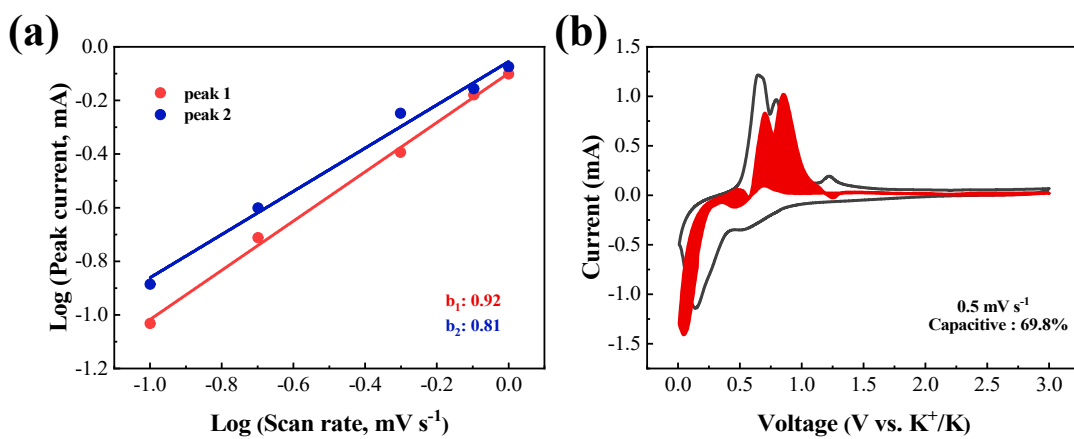


**Figure S16.** a) The corresponding  $b$  values in linear regression. b) The composition of pseudocapacitive characteristics in the CV curve at a scan rate of  $0.5 \text{ mV s}^{-1}$ .



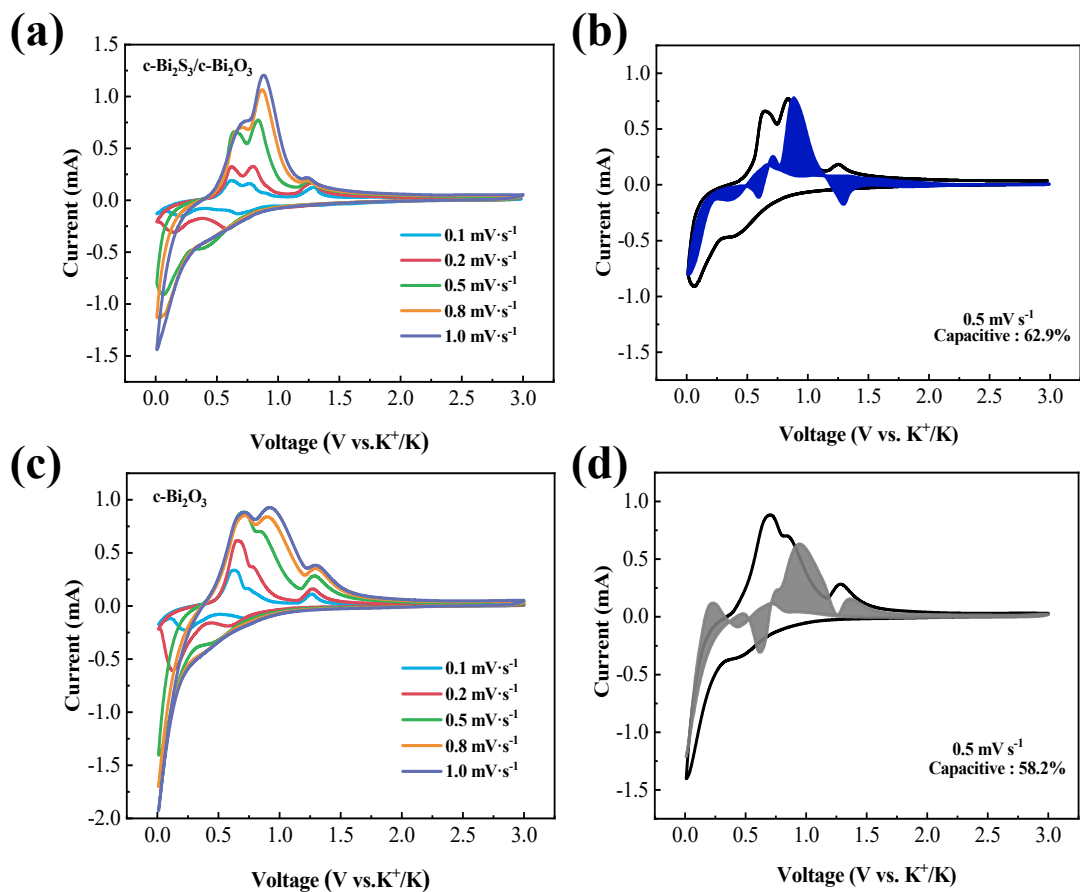


**Figure S17.** a,c) CV curves of c-Bi<sub>2</sub>S<sub>3</sub>/c-Bi<sub>2</sub>O<sub>3</sub> and c-Bi<sub>2</sub>O<sub>3</sub> at different sweeping rates. b,d) The contribution ratio of pseudocapacitive characteristics of c-Bi<sub>2</sub>S<sub>3</sub>/c-Bi<sub>2</sub>O<sub>3</sub> and c-Bi<sub>2</sub>O<sub>3</sub> in the CV curve at a scan of 0.5 mV s<sup>-1</sup>.

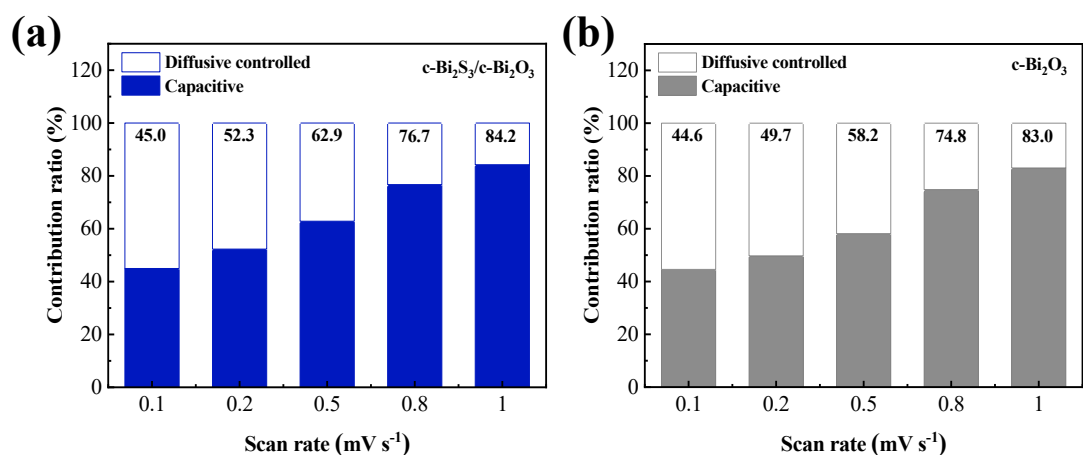


**Figure S18.** a,b) The contribution ratio of surface-controlled and diffusion-controlled behaviors of c-Bi<sub>2</sub>S<sub>3</sub>/c-Bi<sub>2</sub>O<sub>3</sub> and c-Bi<sub>2</sub>O<sub>3</sub> at different scan rates.

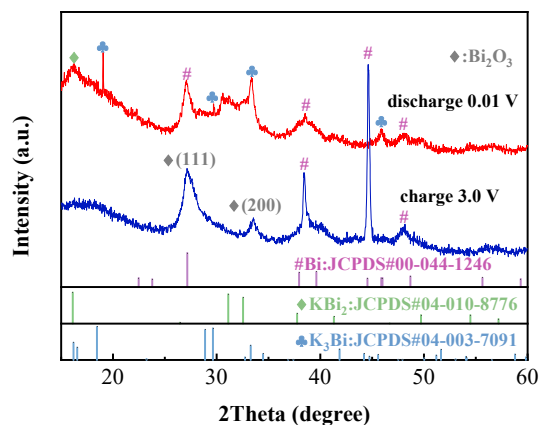


**Figure S19.** Ex-situ XRD patterns of a-Bi<sub>2</sub>S<sub>3</sub>/c-Bi<sub>2</sub>O<sub>3</sub> electrode during the first discharge and charge.

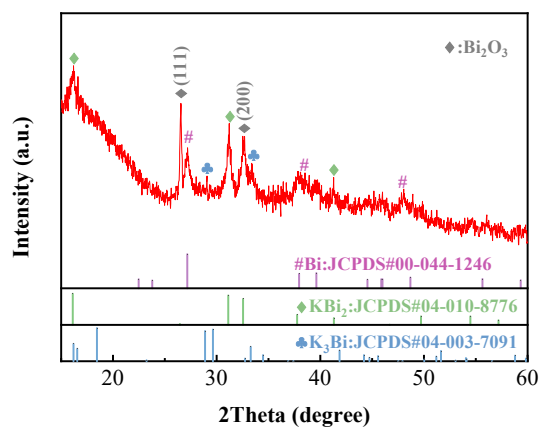


**Figure S20.** XRD patterns of a-Bi<sub>2</sub>S<sub>3</sub>/c-Bi<sub>2</sub>O<sub>3</sub> electrode after 300 cycles.

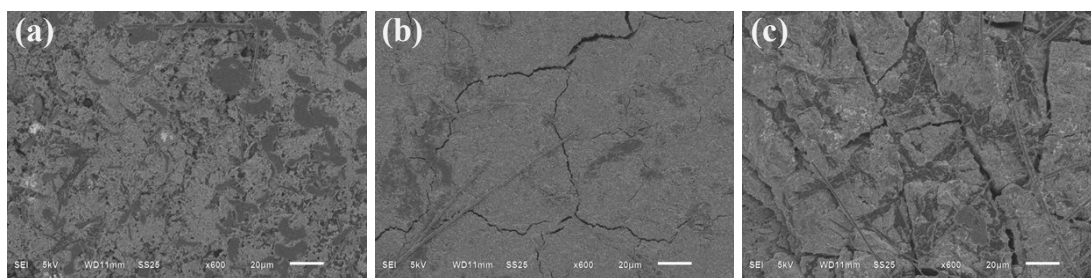


**Figure S21.** The post-mortem SEM images of a) a-Bi<sub>2</sub>S<sub>3</sub>/c-Bi<sub>2</sub>O<sub>3</sub>, b) c-Bi<sub>2</sub>S<sub>3</sub>/c-Bi<sub>2</sub>O<sub>3</sub> and c) c-Bi<sub>2</sub>O<sub>3</sub>.

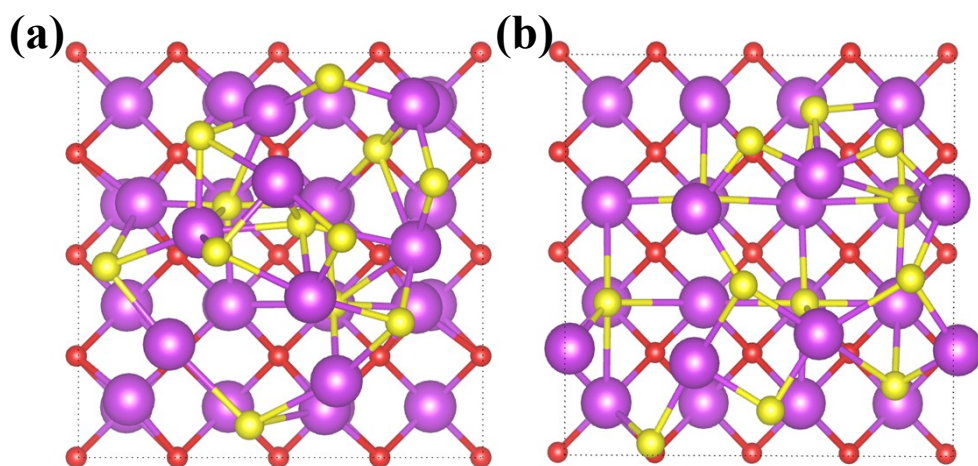


**Figure S22.** Top views of the optimized structure a)  $a\text{-Bi}_2\text{S}_3/c\text{-Bi}_2\text{O}_3$  and b)  $c\text{-Bi}_2\text{S}_3/c\text{-Bi}_2\text{O}_3$ .

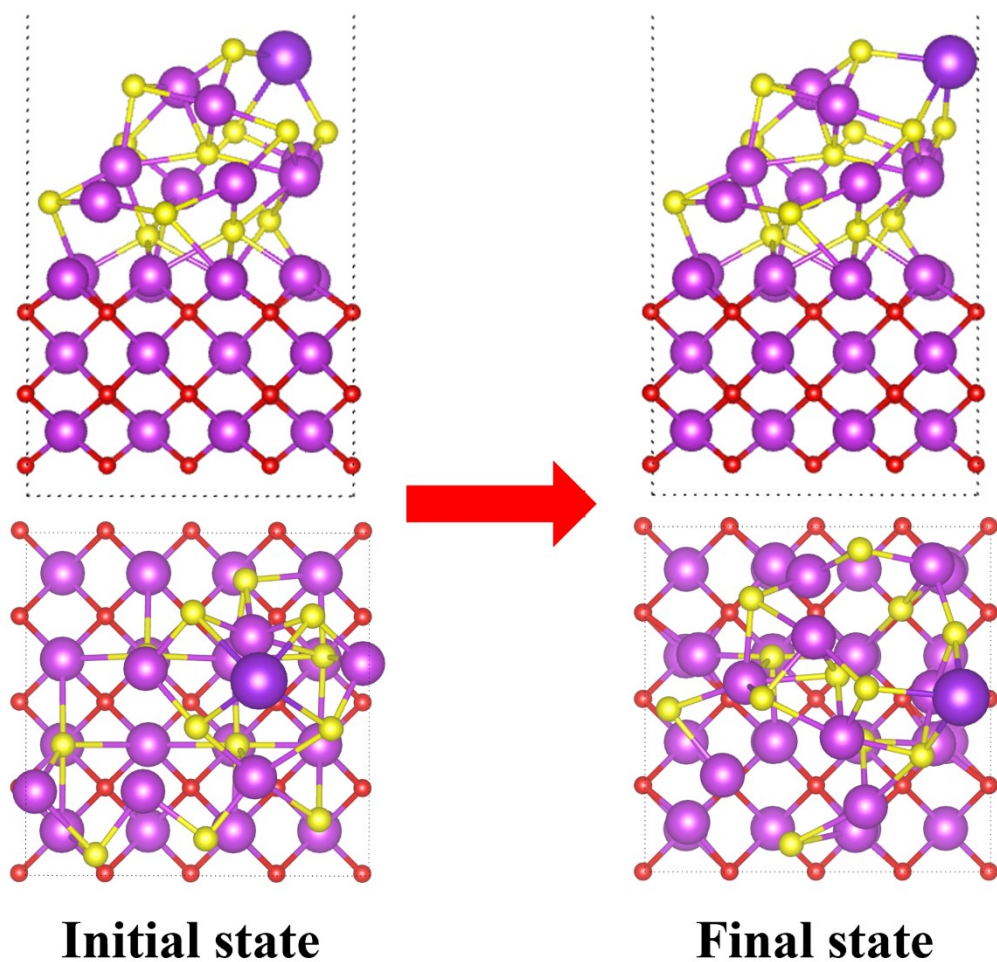


**Figure S23.** The initial and final state of K-atom diffusion in  $a\text{-Bi}_2\text{S}_3/c\text{-Bi}_2\text{O}_3$ .

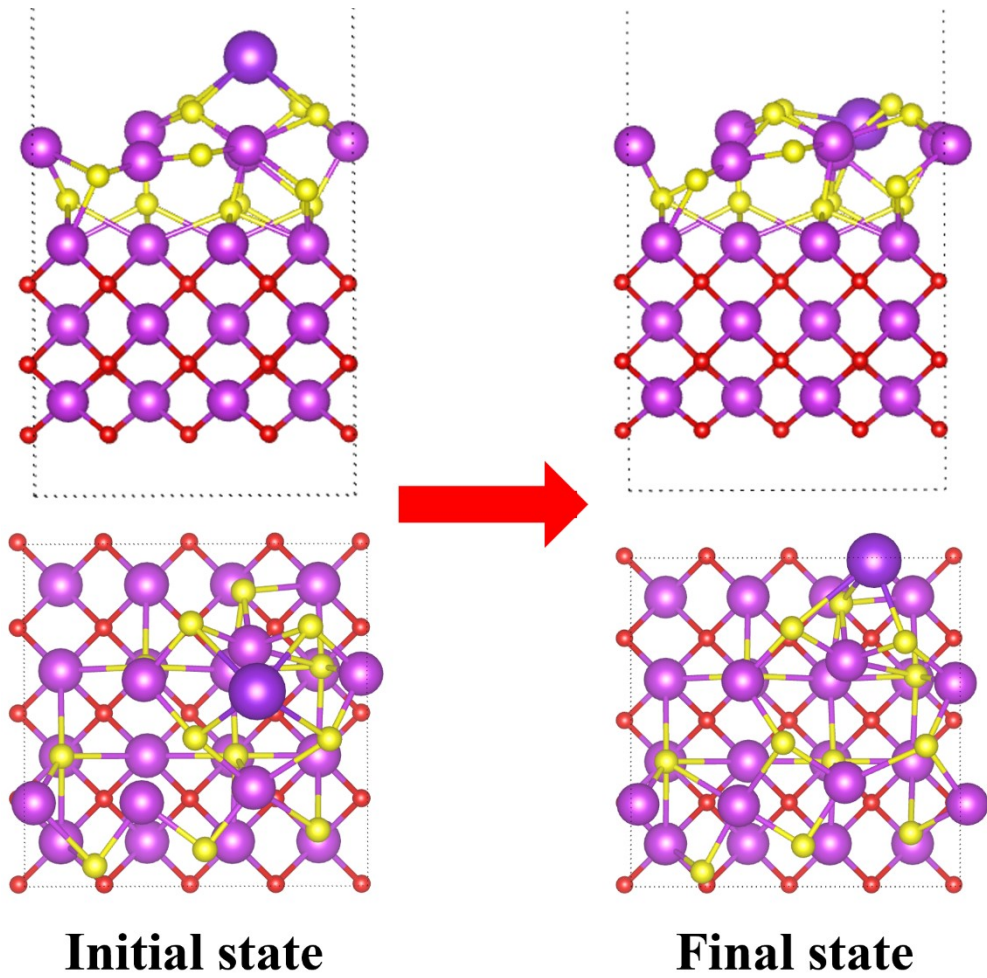


**Figure S24.** The initial and final state of K-atom diffusion in c-Bi<sub>2</sub>S<sub>3</sub>/c-Bi<sub>2</sub>O<sub>3</sub>.

## References

1. P. E. Blochl, *PHYSICAL REVIEW B*, 1994, **50**, 17953-17979.
2. M. Yu and D. R. Trinkle, *JOURNAL OF CHEMICAL PHYSICS*, 2011, **134**.